Analysis of Tornadogenesis Failure Using Rapid-Scan Data from the Atmospheric Imaging Radar

KYLE D. PITTMAN*

Department of Geographic and Atmospheric Sciences, Northern Illinois University
DeKalb, Illinois

ANDREW MAHRE

School of Meteorology, and Advanced Radar Research Center, University of Oklahoma
Norman, Oklahoma

DAVID J. BODINE AND CASEY B. GRIFFIN

Advanced Radar Research Center, University of Oklahoma
Norman, Oklahoma

ABSTRACT

Tornadogenesis in supercell thunderstorms has been a heavily studied topic by the atmospheric science community for several decades. However, the reasons why some supercells produce tornadoes, while others in similar environments and with similar characteristics do not, remains poorly understood. For this study, tornadogenesis failure is defined as a supercell appearing capable of tornado production, both visually and by meeting a vertically contiguous differential velocity (ΔV) threshold, without producing a sustained tornado. Data from a supercell that appeared capable of tornadogenesis (but which failed to produce a sustained tornado) was collected by the Atmospheric Imaging Radar (the AIR, a high temporal resolution radar) near Denver, CO on 21 May 2014. These data were examined to explore the mechanisms of tornadogenesis failure within supercell thunderstorms. Analysis was performed on the rear-flank downdraft (RFD) region and mesocyclone, as previous work highlights the importance of these supercell features in tornadogenesis. Preliminary results have found a lack of vertical continuity in rotation between the lowest level of data analyzed (100 m AGL), and heights aloft ($>$ 500 m AGL). A relative maximum in ΔV occurred approximately 100 m AGL ($0.5°$ in elevation on the radar) around the time of suspected tornadogenesis failure; this contrasts with weaker ΔV at elevations aloft. Additionally, the RFD produced by the Denver Supercell had a peak in intensity aloft (between 2.5 and 3 km in height) just prior to the time of tornadogenesis failure, while simultaneously experiencing a relative minimum in intensity in the layer between the ground and 1 km.

1. Introduction

Tornadoes have been intensely studied for several decades, due to the potential for significant harm to life and property they can produce. Tornado production in supercell thunderstorms has been of particular interest, because the majority of tornadoes (and the vast majority of all violent tornadoes) in the United States are produced by supercells (Doswell and Burgess 1993; Trapp et al. 2005b). Many significant scientific advances in the understanding of tornadoes have taken place in the last 50 years, due to advances in computational technology and numerous, well-documented observations of tornadoes (Doswell

and Burgess 1993; French et al. 2013, 2014). Some factors relating to tornado formation, such as the cause of deep, persistent, rotating updrafts in supercell thunderstorms (mesocyclones) (Lemon and Doswell 1979; Davies-Jones 1984; Rotunno and Klemp 1985), or the environments conducive to supercell and tornado production (Rasmussen and Blanchard 1998; Thompson et al. 2003; Craven and Brooks 2004) are well-understood. However, despite being a heavily researched topic, the actual mechanisms that cause tornadogenesis are still not fully known (Markowski and Richardson 2009, 2010; French et al. 2013).

An important part of understanding tornadogenesis is determining what causes this process to fail in some storms. Trapp (1999) defined tornadogenesis failure as a moderate-to-strong mesocyclone within the lowest several hundred meters above the ground, which qualitatively

---

Corresponding author address: Kyle Pittman, Department of Geographic and Atmospheric Sciences - Northern Illinois University, 1425 Lincoln Hwy, DeKalb, IL 60115
E-mail: kpittman@niu.edu

appears capable of tornadogenesis, yet does not produce a tornado. There have been numerous documented cases where supercell thunderstorms with deep, persistent mesocyclones in seemingly favorable synoptic and mesoscale environments fail to produce a tornado; per the work of Trapp et al. (2005a), only around 26 percent of mesocyclones end up producing tornadoes. An intense mesocyclone (with observed ΔV of 118 m s^{-1}) occurred with a supercell near Superior, NE on 22 June 2003, yet failed to produce a tornado (Wakimoto et al. 2004). The fact that a mesocyclone within the lowest kilometer above the ground is not a sufficient indicator of tornadogenesis makes issuing accurate tornado warnings difficult. Brooks et al. (1993) noted that "establishing why mesocyclones fail to produce significant tornadoes can reduce the possibility of high false alarm rates [of issued tornado warnings] based on radar signatures of mesocyclones". For this study, tornadogenesis failure is defined as a storm which a) appears qualitatively capable of tornado production from visual observations (Bluestein 1999), and b) has vertically continuous rotation at or below the low-level mesocyclone (with a ΔV intensity of 35 m s^{-1}), but does not produce a sustained tornado. This is a slight modification to the definition of tornadogenesis failure presented in Trapp (1999). That study used vertical vorticity calculations within the lowest several hundred meters as a measure of mesocyclone strength. However, because high temporal resolution radar data was used in this study, a more radar specific threshold was used to define mesocyclone intensity strength.

While previous work such as Trapp (1999) has investigated possible modes of tornadogenesis failure, high temporal-resolution radar data have not yet been used to examine tornadogenesis failure. Previous studies of tornadoes have shown that radar observations at high temporal-resolution are necessary, because of the rapidly evolving behavior tornadoes exhibit from birth and decay (Bluestein et al. 2003; Wurman et al. 2007; French et al. 2013; Houser et al. 2015; Mahre et al. 2018; Griffin et al. 2019). The Atmospheric Imaging Radar (AIR) is a rapid-scan, mobile phased array imaging radar developed by the Advanced Radar Research Center at the University of Oklahoma (Isom et al. 2013; Kurdzo et al. 2017), and has the ability to obtain full volumetric scans of a supercell thunderstorm in 10 s or less. This is a time scale necessary for effective observations to be taken that can provide further insight on tornado development (Bluestein et al. 2010; Houser et al. 2015). More details will be discussed on the AIR in the data section of this paper.

This study examines a dataset collected by the AIR from a suspected tornadogenesis failure case within a supercell thunderstorm on 21 May 2014. This study only examines a tornadogenesis failure case from a supercell thunderstorm; no attempt in this study is made to examine tornadogenesis failure by any non-supercellular thunderstorm (i.e., quasi-linear convective system induced tornadoes or landspouts/waterspouts). The environment the storm formed in, along with associated tornado reports and visual observations, are also examined. The goal of this work is to identify any specific spatial and/or temporal patterns in the mechanisms involved in tornadogenesis failure for this case. By using different analysis techniques to contrast the high temporal resolution radar data with the storm environment and associated storm reports, a better understanding of mechanisms and causation of tornadogenesis failure could be achieved.

Section 2 of this study describes the AIR in further detail, and also introduces the details of the tornadogenesis failure case which will be analyzed in this study. Section 3 discusses the quality control and analysis methods used on the data. Results and interpretation of these data analysis techniques are discussed in Sections 4 and 5, respectively. Future work that will be completed on this study (outside the scope of the 2019 REU program) is also addressed.

2. Data

a. The Atmospheric Imaging Radar

The AIR is a rapid-scan, X-band (3.14 cm wavelength) mobile phased array imaging radar, which was developed and built by the Advanced Radar Research Center (ARRC) at the University of Oklahoma ((Isom et al. 2013; Kurdzo et al. 2017). Imaging radars collect data by transmitting a wide beam of electromagnetic energy; in the case of the AIR, this is 20° in elevation by 1° in azimuth. Some of the electromagnetic energy from the transmit beam is backscattered by hydrometeors, which is collected by 36 individual receivers on the AIR's antenna. A post-processing software method called digital beamforming (DBF) allows for 20 individual 1° by 1° elevation angles to be reconstructed simultaneously from the received electromagnetic energy, precluding the need to account for vertical advection (Skolnik 2001; Isom et al. 2013; Kurdzo et al. 2017). These simultaneously received images are known as RHIs (Range Height Indicators), and are collected with each pulse of energy sent and received by the radar. The beam is mechanically steered in azimuth across the area of interest, thus allowing for rapid temporal three dimensional volumetric data collection possibilities with the AIR. New scan volumes displaying reflectivity, velocity, and spectrum width data can be obtained in 10 s or less with this method. Additional details about the AIR can be found in Isom et al. (2013), and further details on its observations of supercells and tornadoes can be found in Kurdzo et al. (2017).

b. Dataset

The dataset was obtained on the afternoon of 21 May 2014, from a supercell thunderstorm which formed just
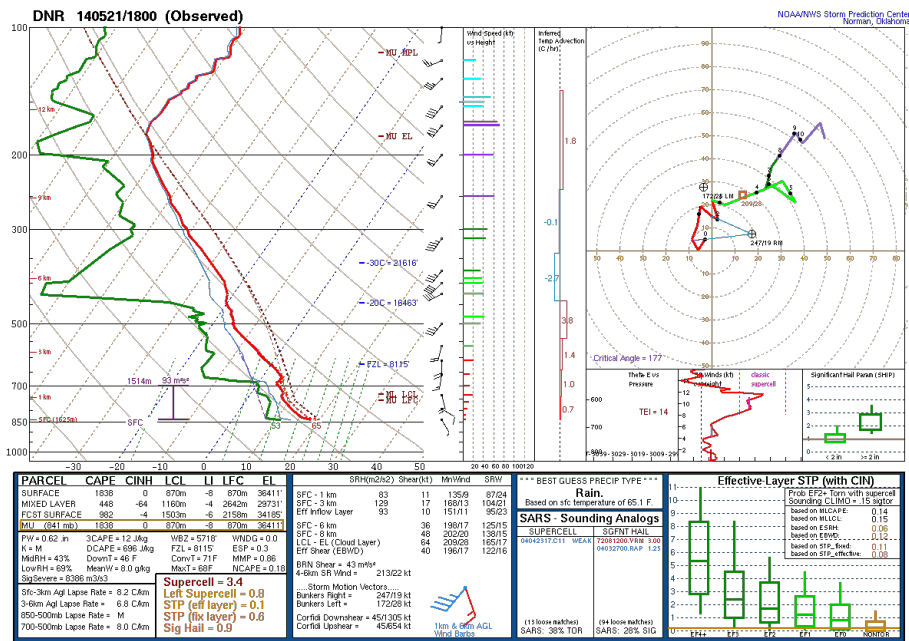
FIG. 1: The 18:00 UTC observed sounding from KDNR. This was the closest observed upper air sounding available for this storm, launched within 10 km from the initiation location of the storm and 2.5 hours prior to the AIR deployment. Note the overall veering tropospheric wind profile, and favorable surface based parcel environment.

east of Denver, CO. The approximate AIR deployment time was from 20:25:44 to 20:33:21 UTC[1]. 54 individual volume scans were obtained by the AIR during this deployment. The AIR was located approximately between 12 km (20:25) and 9 km (20:33) due east of the mesocyclone's location (as denoted by radar) during the deployment. Data were analyzed at the 0.5°, 2.5°, 4.0°, 7.0°, 10.0°, 12.0°, and 15.0° elevation angles.

The supercell formed in a moderately unstable thermodynamic environment (1500-2000 J kg^{-1} of CAPE), which was combined with a veering tropospheric wind profile (Figure 1). The environment became more favorable as the afternoon progressed, as diurnal heating increased instability in the area[2]. Southeasterly upslope flow over central CO advected low to mid 50F dewpoints into the region, along with enhanced low-level wind shear due to the Denver Convergence Vorticity Zone (DCVZ).

The DCVZ (Szoke et al. 2006) is a localized mesoscale wind pattern, usually with a north-south orientation and 50-100 km long, which forms with regularity to the east of the Denver Metropolitan Area. Convergent flow favorable to the development of low-level vorticity develops in this area, because of southerly low-level winds intersecting an east-west oriented topographic ridge (known as the Palmer Divide). When upslope southeasterly flow is present in a favorable thermodynamic atmosphere in this region, it can lead to supercell thunderstorm initiation and an increased likelihood of tornadogenesis.

The storm initiated over Denver around 19:15 UTC, and obtained supercellular characteristics on radar as it moved eastward through Aurora, CO over the next hour (Figure 2). In addition to the increased low-level shear from the DCVZ, the storm was likely also impacted by an approaching outflow boundary left over from nocturnal thunderstorms in northeast CO. This additional boundary interaction is significant, as previous studies have shown the importance of boundary interactions on tornado production in supercells (Maddox et al. 1980; Markowski et al. 1998). Visual observations of the storm taken near the time of the AIR deployment also indicated the storm possessed attributes common to storms capable of tor-

---

[1]It should be noted that the UTC time of the AIR deployment is considered approximate, as it may not match up exactly to the UTC time logged on the tornado reports or photographs examined in this study.

[2]Environment data for this severe event was accessed from the Storm Prediction Center's Severe Weather Events Archive data, and can be found at https://www.spc.noaa.gov/exper/archive/event.php?date=20140521.
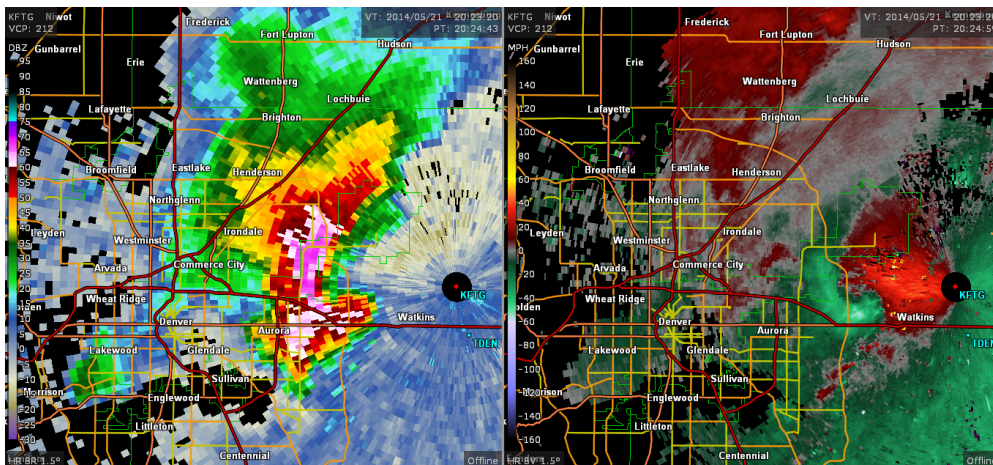
FIG. 2: Denver/Boulder, CO (KFTG) WSR-88D Reflectivity and Radial Velocity imagery (1.5° elevation scan) of the Denver Supercell at 20:23:20 UTC, showing the well-defined tornadic supercell radar characteristics (Lemon 1977; Forbes 1981) the storm had developed at this time (144 seconds before the AIR deployment began). Radar imagery displayed on Gibson Ridge Level III software, with data obtained from the NOAA's National Climatic Data Center archive.

FIG. 3: Image of the rotating wall cloud produced by the Denver Supercell, taken at 20:02 UTC approximately 16.5 km east of the AIR's deployment location. Photo courtesy of Bill Reid.

nado production. Figure 3 shows the lowered, rotating wall cloud produced by this supercell approximately 25 minutes prior to the AIR deployment (cloud base (LCL) heights were estimated to be around 1000 meters per the archived SPC mesoanalysis data). Filtered tornado reports from the Storm Prediction Center (SPC) for 21 May 2014

had 5 reported tornadoes in the area of the supercell, beginning at 20:10 UTC and ending at 20:45 UTC (within +/- 15 minutes of the first and last scan times from the AIR, respectively). One of the reports was located near the rotating wall cloud at 20:30 UTC, during the AIR deployment, and an additional image of a funnel cloud was

FIG. 4: Image of the funnel cloud produced by the Denver Supercell, taken around 20:30 UTC approximately 7 km northwest of the AIR's deployment location during this time. Photo courtesy of Brad Nelson.

captured near this time and location (Figure 4). However, no tornado damage was reported in the area by the local National Weather Service office (Boulder, CO). Given that the storm took place in a synoptically favorable environment, that the storm appeared qualitatively capable of producing a tornado, and that the storm showed strong rotation within the mesocyclone (yet did not produce damage observed at the surface), the storm is considered a case of tornadogenesis failure.

3. Methods

a. Data Issues and Quality Control

Raw data collected by the AIR are subject to a variety of errors, including velocity aliasing, vertical sidelobes, grating lobes, ground clutter, and radio frequency interference. These issues must be accounted for prior to other analysis techniques being performed. Aliased velocity data occurs when the maximum unambiguous velocity (also known as the Nyquist Velocity) that the radar can detect is lower than the true radial velocity; for the case analyzed in this study, the Nyquist velocity is 25 m s^{-1} (Kurdzo et al. 2017). Vertical side lobes on data collected by the AIR are a result of the single $20°$x $1°$ transmit beam pattern; this causes contamination of velocities in areas of low reflectivity from areas of higher reflectivity. Grating lobes are a result of ambiguity in the direction where the antenna is performing digital beamforming on backscattered energy. Other minor data quality issues such as ground clutter (echoes from targets on the ground, mainly within 2 km of the radar's location), or radio frequency interference

(caused by electromagnetic energy of a similar wavelength from another source being backscattered by the same objects) are also present in many of the volume times.

Solo3, a comprehensive radar data editing software developed by the National Center for Atmospheric Research (NCAR), was utilized to correct for the aforementioned data quality issues (Figure 5) that were encountered with raw radar data. First, the reflectivity and velocity data values were filtered with technique called thresholding. This allowed for reflectivity and velocity values which were a result of vertical side lobe and grating lobe issues to be eliminated in areas of interest (the area adjacent to the mesocyclone). This technique removed any data where reflectively was below 25 dBZ. Additional thresholding was performed that removed reflectivity below 30 dBZ in areas not adjacent to the mesocyclone or RFD (in order to clarify the data). Velocity data were manually dealiased for each volume scan at every elevation angle analyzed in the study, in order to reveal true recorded velocity values and help better identify storm features on radar that are associated with tornadogenesis (Lemon 1977).

b. Analysis Methods

Once data had been quality controlled, plan position indicator (PPI) images of reflectivity and velocity data were animated, in order to qualitatively analyze the evolution of storm features with time at each elevation angle. [3] Each

---

[3]Animations of AIR data for the full deployment at every elevation angle analyzed in this study is available at https://sites.google.com/view/kylepittman/research-projects
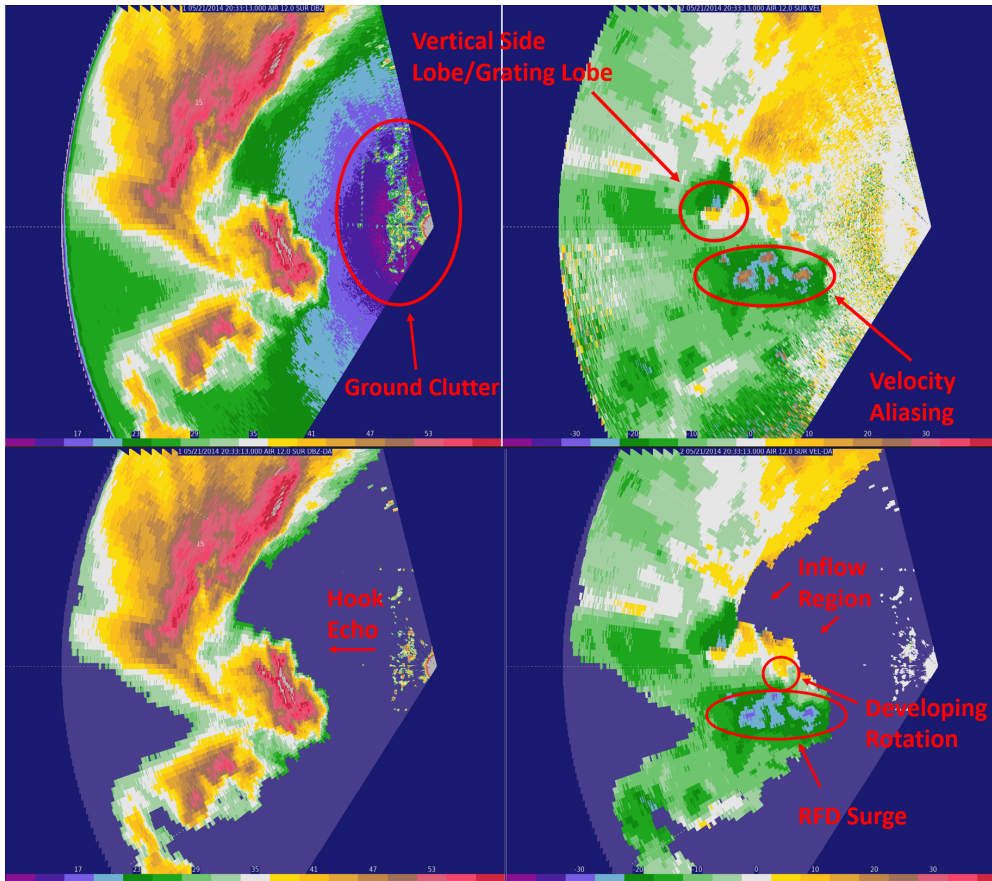
FIG. 5: Example of reflectivity and radial velocity data 12° elevation angle before (top) and after (bottom) corrections to the raw radar data have been made. These data issues must be corrected for on each data volume at every elevation before analysis can be performed. Once corrected, several radar characteristics of tornadic supercells (Lemon 1977; Forbes 1981) are more easily identified.

volume scan at each elevation angle was manually examined for areas of rotation, and to record the location and intensity of velocities associated with the RFD. A time-height plot of radial velocities observed within the RFD during the entire AIR deployment period was created in order to visualize how the intensity of the RFD changed with time. Additionally, a ΔV analysis was performed to examine areas of rotation observed in velocity data during the entire deployment. Similar to the method used in Griffin et al. (2019), values of ΔV are calculated by subjectively selecting centers of rotation on the radial velocity data. A 500-m radius extended from the selected center of rotation, which logged maximum and minimum velocity values. In order to mitigate potential errors in calculation, all centers of rotation were visually inspected multiple times. By using this analysis method, it is possible to quantify and visually plot how areas of rotation change in intensity with time and height as the storm progresses.

4. Results

A strong RFD surge greater than 20 m s^{-1} for all volumes is another notable feature observed within the well-defined hook echo for the Denver Supercell. The hook echo has long been a radar characteristic associated with tornadic supercells (Lemon 1977; Forbes 1981). The hook echo and high radial velocity values within the RFD region are visible at all of the elevation angles of data analyzed from the AIR deployment on this storm. Because the radar beam is roughly aligned with the direction of winds within the RFD, these single Doppler estimates recorded by the AIR are expected to be close to the true RFD winds. The time-height plot shown in Figure 6 reveals that the most intense RFD radial velocity values (greater than 35 m s^{-1}) are confined to elevations higher than 1.5 km AGL, occurring between 20:27:06 and 20:30:30 UTC. In contrast, radial velocities below the approximate cloud base (1000 m) decrease as the deployment progresses, to less than 25
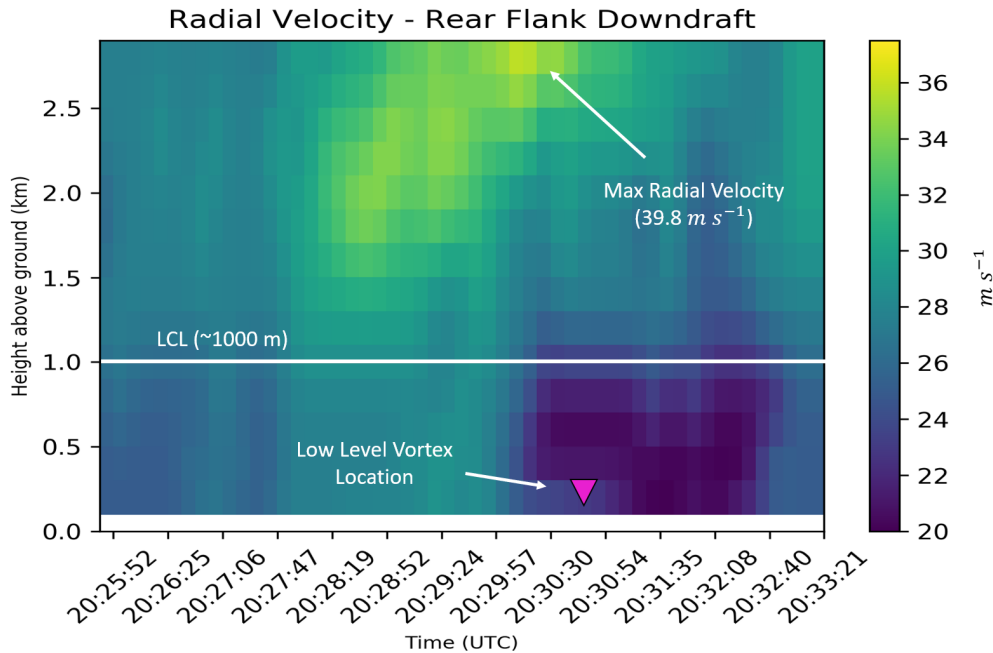
FIG. 6: Time-height plot of RFD velocities for the entire duration of the entire AIR deployment for the Denver Supercell. Data is plotted for the 7 analyzed elevation angles, however to create a plot that provides better visual representation of changes with time and height, uses methods of linear interpolation and Gaussian smoothing to every 200 m. Constant elevations calculated for an average beam height are used for this plot; it should be noted that the height at which the radar beam intersects storm features gets lower with time as the storm gets closer to the radar throughout the course of the deployment.

m s^{-1} for volumes after 20:29:24 UTC, and occur immediately following the most intense RFD velocities aloft. Throughout the column, RFD winds decrease almost simultaneously after 20:30:30 UTC. Interestingly, this large contrast of radial velocity values between high and low elevations occurs within approximately 30 seconds of the maximum intensity of ΔV at the surface, shown in Figure 8. It should be noted that the spatial extent of the intense RFD velocities is also constantly changing with time throughout the AIR deployment, as shown in at the 4° and 10° elevation angles in Figure 7.

Figure 8 shows the results of the ΔV analysis for all 7 elevations of data which were analyzed in the study. It can be seen from this plot that the most intense areas of ΔV (greater than 35 m s^{-1}) never fully align with time or height at any point during the deployment, showing quantitatively the failure of sustained tornadogenesis within this storm. Interestingly, a peak in ΔV of 38.5 m s^{-1} is observed near the surface between 20:30:30 and 20:30:54 UTC, which approximately aligns to the time of the aforementioned tornado report at 20:30 UTC, and with the funnel cloud observed (Figure 4). There is also an apparent surge in mesocyclone intensity, with several volumes of ΔV exceeding 35 m s^{-1} observed at the 12° and 15° ele-

vations, from 20:28:19 to 20:29:57 UTC. Along with the contrast of radial velocity values at different elevations observed in the RFD, this intensification period precedes the maximum intensity of ΔV at the surface by approximately 30 seconds. Based on the results shown in Figure 8, there also does not appear to be any direct vertical continuity between these two areas of rotation.

5. Discussion

The results shown in Figure 6 are significant, as the contrast in higher radial velocity values aloft (simultaneously occurring at the time of tornadogenesis failure) with lower values at the surface implies horizontal shear in the region of the RFD. In the case of the Denver Supercell, it appears that the RFD was unable to generate the required amount of vertical vorticity near the surface for tornadogenesis to occur. The inherent limitation of this analysis is that it only considers 7 elevations of data to analyze the layer between the surface and 3 km; additional analysis at every elevation of data collected by the AIR (from 0.5° to 20°) would need to be performed before a definite conclusion can be reached on this observation. These results are interesting when considering that current theory suggests that an RFD is not required for tornadogenesis when preexisting
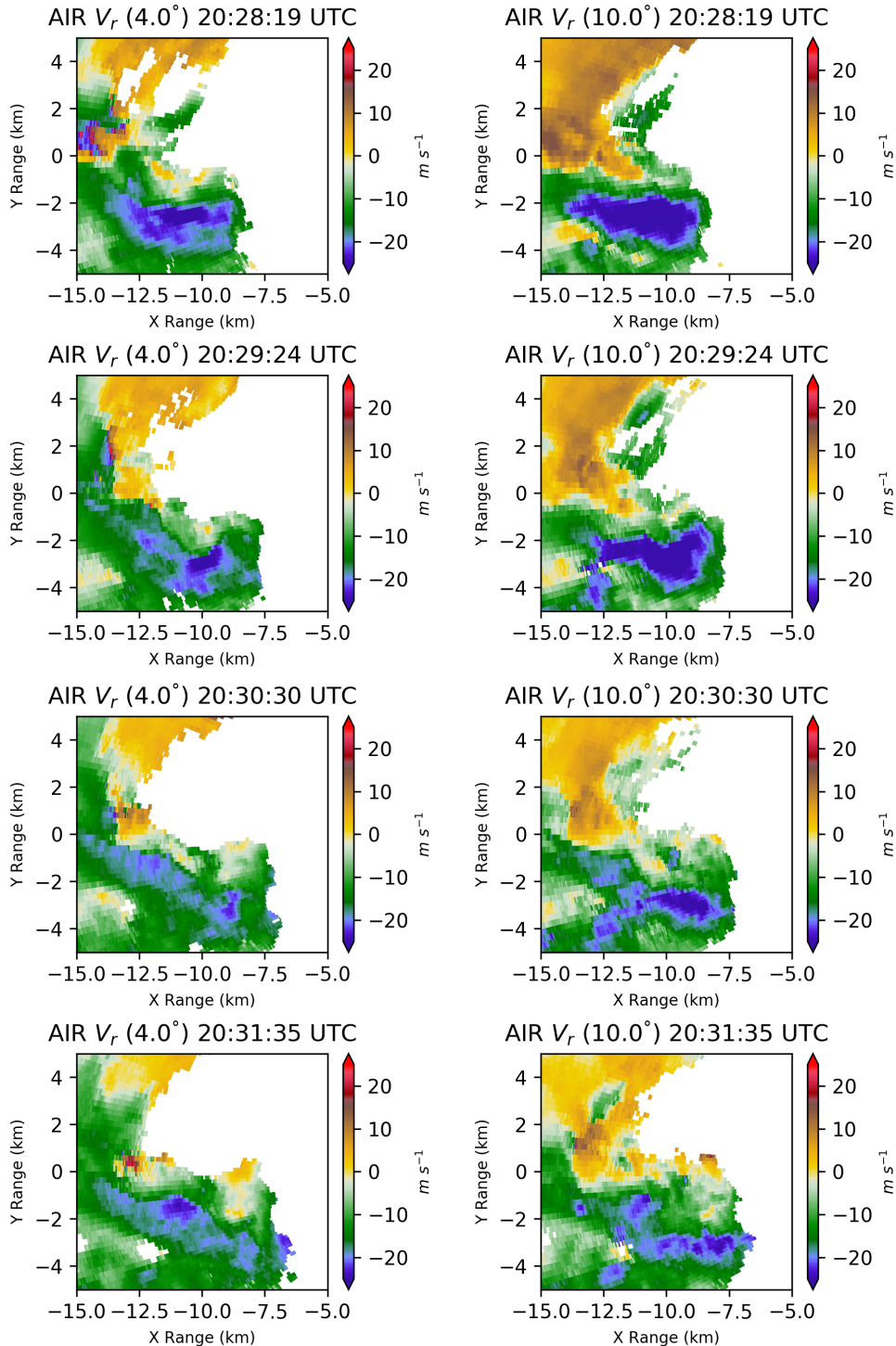
FIG. 7: AIR radial velocity data at the $4°$ and $10°$ elevation angles, for 4 different volumes from 20:28:19 UTC to 20:29:57 UTC. Note the constantly changing spatial extent of the RFD thoughout the deployment.
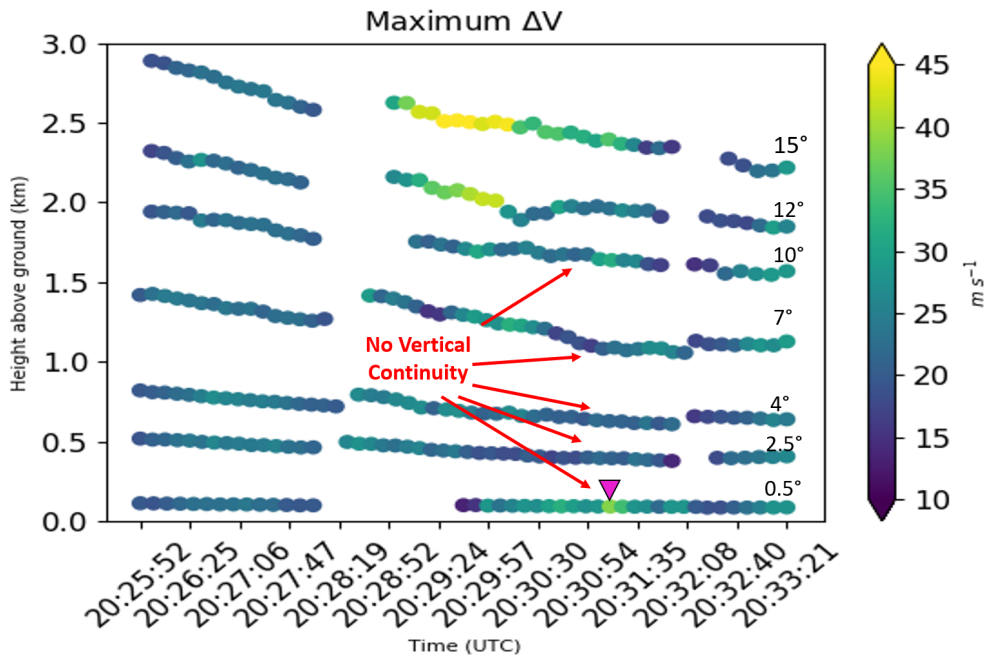
FIG. 8: As in figures 5 and 12 in Houser et al. (2015), plot of maximum ΔV for vortices observed at all 7 analyzed elevation angles for the entire duration of the AIR deployment. The maximum magnitude of ΔV is shown by the color (m s^{-1}). The approximate time of the tornado report which corresponds with increased low-level rotation is noted on the image.

vertical vorticity is located near the ground (Markowski and Richardson 2009), which may have been present in the case of the Denver Supercell, when considering the DCVZ and approaching outflow boundary. It is possible that strong RFD winds interacting with the mesocyclone could have produced excessive tilting, which prevented tornadogenesis from occurring. However, more analysis would have to be completed in order to verify this hypothesis.

Another significant observation from the results is the lack of vertical continuity in rotation at different analyzed elevation angles, best shown by Figures 8 and 9. Despite the increase in ΔV associated with the mesocyclone aloft, rotation at subsequent levels beneath it was not able to connect to the slight increase in ΔV observed at the 0.5° elevation angle around the time of the observed funnel cloud. Current theories on tornadogenesis have shown that vertical continuity in rotation beneath the mesocyclone is required for tornadogenesis (Markowski and Richardson 2010; French et al. 2013). The presence of low-level vortices developing below the mesocyclone was not a precursor to a sustained tornado in this case study, as none of these were able to achieve vertical continuity and develop into a sustained tornado. It should be noted that this finding is also limited because only 7 elevations of radial velocity data were analyzed in this study; additional data

needs to be examined in order to get a better understanding of the vertical extent of rotation near the mesocyclone.

6. Future Work

In addition to analyzing more elevations of data collected by the AIR during this deployment, it may also be possible to perform a dual-Doppler analysis on the Denver Supercell, because of the close proximity in which it occurred with the Denver/Boulder, CO, Weather Surveillance Radar-1988 Doppler (WSR-88D) and the Denver International Airport Terminal Doppler Radar. Previous work on tornadoes has shown that dual-Doppler analysis can be useful in further analyzing the updrafts and downdrafts associated with tornadic supercells (Wurman et al. 2007; Tanamachi et al. 2012). The same quality control and analysis techniques used in the Denver Supercell will be performed on two additional cases of tornadogenesis failure collected by the AIR in 2017 near McLean, TX (on 16 May) and Waynoka, OK (18 May). These 3 cases will also be compared to each other to examine possible similarities or differences in the modes of tornadogenesis failure. Additionally, the analysis performed on the 3 tornadogenesis failure cases should be compared to a case of tornadogenesis collected by the AIR on 23 May 2016
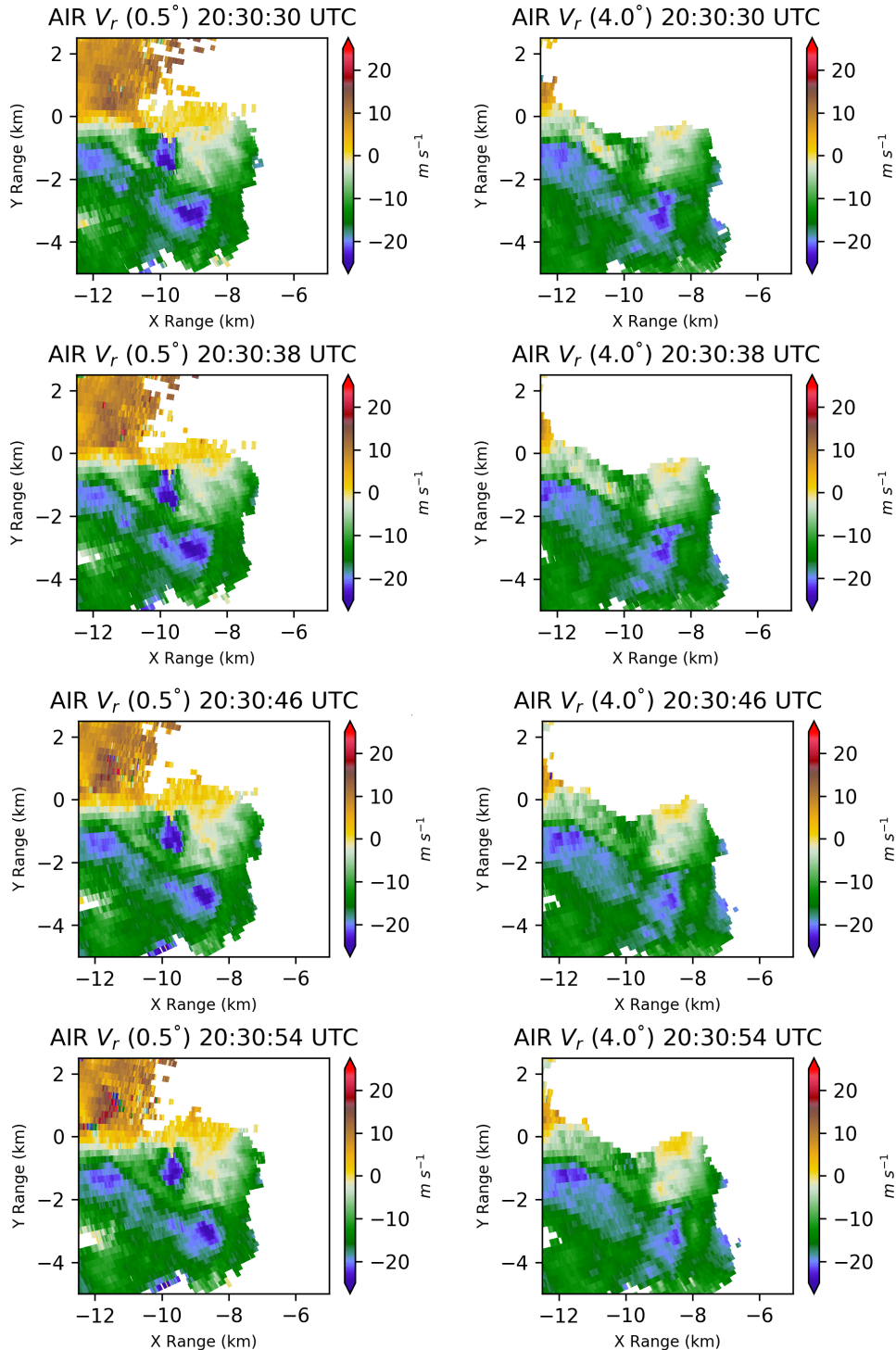
FIG. 9: AIR radial velocity data at the 0.5° and 4° elevation angles, from 20:30:30 - 20:30:54 UTC. This corresponds to times the maximum in low-level ΔV is observed in Figure 8, and shows the lack of rotation at higher elevations.

near Woodward, OK (Griffin et al. 2016), again to examine possible similarities or differences in the mechanisms which are responsible for the observed phenomena of each case.

References

Bluestein, H. B., 1999: A history of severe-storm-intercept field programs. *Wea. Forecasting*, **14**.

Bluestein, H. B., M. M. French, I. PopStefanija, R. T. Bluth, and J. B. Knorr, 2010: A mobile, phased-array doppler radar for the study of severe convective storms. *Bull. Amer. Meteor. Soc.*, **91**.

Bluestein, H. B., C. C. Weiss, and A. L. Pazmany, 2003: Mobile doppler radar observations of a tornado in a supercell near Bassett, Nebraska, on 5 June 1999. Part I: Tornadogenesis. *Mon. Wea. Rev.*, **131**.

Brooks, H. E., C. A. Doswell III, and R. Davies-Jones, 1993: Environmental Helicity and the Maintenance and Evolution of Low-Level Mesocyclones. The Tornado: Its Structure, Dynamics, Prediction, and Hazards. *Geophys. Monogr.*, **79**, 97–104.

Craven, J., and H. Brooks, 2004: Baseline climatology of sounding derived parameters associated with deep, moist convection. *Natl. Weather Dig.*, **28**, 13–24.

Davies-Jones, R., 1984: Streamwise vorticity: The origin of updraft rotation in supercell storms. *J. Atmos. Sci.*, **41**.

Doswell, C. A., and D. W. Burgess, 1993: Tornadoes and tornadic storms: A review of conceptual models. *Geophys. Monogr.*

Forbes, G. S., 1981: On the reliability of hook echoes as tornado indicators. *Mon. Wea. Rev.*, **109**.

French, M. M., H. B. Bluestein, I. PopStefanija, C. A. Baldi, and R. T. Bluth, 2013: Reexamining the vertical development of tornadic vortex signatures in supercells. *Mon. Wea. Rev.*, **141**.

French, M. M., H. B. Bluestein, I. PopStefanija, C. A. Baldi, and R. T. Bluth, 2014: Mobile, phased-array, doppler radar observations of tornadoes at X band. *Mon. Wea. Rev.*, **142**.

Griffin, C., D. Bodine, J. Kurdzo, R. Palmer, A. Mahre, J. Lujan, and A. Byrd, 2016: High-temporal resolution observations of the 23 May 2016 Woodward, OK, Tornadic Supercell using the Atmospheric Imaging Radar. *28th AMS Conference on Severe Local Storms, SLS 2016.*

Griffin, C. B., D. J. Bodine, J. M. Kurdzo, A. Mahre, and R. D. Palmer, 2019: High-temporal resolution observations of the 27 May 2015 Canadian, Texas, tornado using the Atmospheric Imaging Radar. *Mon. Wea. Rev.*, **147**.

Houser, J. L., H. B. Bluestein, and J. C. Snyder, 2015: Rapid-scan, polarimetric, doppler radar observations of tornadogenesis and tornado dissipation in a tornadic supercell: The El Reno, Oklahoma Storm of 24 May 2011. *Mon. Wea. Rev.*, **143**.

Isom, B., and Coauthors, 2013: The Atmospheric Imaging Radar: Simultaneous volumetric observations using a phased array weather radar. *J. Atmos. Oceanic Technol.*, **30**.

Kurdzo, J. M., and Coauthors, 2017: Observations of severe local storms and tornadoes with the Atmospheric Imaging Radar. *Bull. Amer. Meteor. Soc.*, **98**.

Lemon, L., 1977: *New Severe Thunderstorm Radar Identification Techniques and Warning Criteria: A Preliminary Report*. 1st ed., National Severe Storms Forecast Center, 64 pp.

Lemon, L. R., and C. A. Doswell, 1979: Severe thunderstorm evolution and mesocyclone structure as related to tornadogenesis. *Mon. Wea. Rev.*, **107**.

Maddox, R. A., L. R. Hoxit, and C. F. Chappell, 1980: A study of tornadic thunderstorm interactions with thermal boundaries. *Mon. Wea. Rev.*, **108**.

Mahre, A., J. M. Kurdzo, D. J. Bodine, C. B. Griffin, R. D. Palmer, and T.-Y. Yu, 2018: Analysis of the 16 May 2015 Tipton, Oklahoma, EF-3 Tornado at high spatiotemporal resolution using the Atmospheric Imaging Radar. *Mon. Wea. Rev.*, **146**.

Markowski, P., and Y. Richardson, 2009: Tornadogenesis: Our current understanding, forecasting considerations, and questions to guide future research. *Atmos. Res.*, **93**, doi:10.1016/j.atmosres.2008.09.015.

Markowski, P., and Y. Richardson, 2010: *Mesoscale Meteorology in Midlatitudes*. 1st ed., Wiley-Blackwell, 407 pp.

Markowski, P. M., E. N. Rasmussen, and J. M. Straka, 1998: The occurrence of tornadoes in supercells interacting with boundaries during VORTEX-95. *Wea. Forecasting*, **13**.

Rasmussen, E. N., and D. O. Blanchard, 1998: A baseline climatology of sounding-derived supercell and tornado forecast parameters. *Wea. Forecasting*, **13**.

Rotunno, R., and J. Klemp, 1985: On the rotation and propagation of simulated supercell thunderstorms. *J. Atmos. Sci.*, **42**.

Skolnik, M., 2001: *Introduction to Radar Systems*. 3rd ed., McGraw-Hill Education, 784 pp.

Szoke, E., D. Barjenbruch, R. Glancy, and R. Kleyla, 2006: The Denver Cyclone and Tornadoes 25 years later: The continued challenge of predicting nonsupercell tornadoes. *23rd AMS Conference on Severe Local Storms, SLS 2006.*

Tanamachi, R. L., H. B. Bluestein, J. B. Houser, S. J. Frasier, and K. M. Hardwick, 2012: Mobile, X-band, polarimetric doppler radar observations of the 4 May 2007 Greensburg, Kansas, Tornadic Supercell. *Mon. Wea. Rev.*, **140**.

Thompson, R. L., R. Edwards, J. A. Hart, K. L. Elmore, and P. Markowski, 2003: Close proximity soundings within supercell environments obtained from the rapid update cycle. *Wea. Forecasting*, **18**.

Trapp, R. J., 1999: Observations of nontornadic low-level mesocyclones and attendant tornadogenesis failure during VORTEX. *Mon. Wea. Rev.*, **127**.

Trapp, R. J., G. J. Stumpf, and K. L. Manross, 2005a: A reassessment of the percentage of tornadic mesocyclones. *Wea. Forecasting*, **20**.

Trapp, R. J., S. A. Tessendorf, E. S. Godfrey, and H. E. Brooks, 2005b: Tornadoes from squall lines and bow echoes. part I: Climatological distribution. *Wea. Forecasting*, **20**.

Wakimoto, R. M., H. Cai, and H. V. Murphey, 2004: The Superior, Nebraska Supercell during BAMEX. *Bull. Amer. Meteor. Soc.*, **85**.

Wurman, J., Y. Richardson, C. Alexander, S. Weygandt, and P. F. Zhang, 2007: Dual-doppler analysis of winds and vorticity budget terms near a tornado. *Mon. Wea. Rev.*, **135**.